Chaos, Solitons and Fractals 174 (2023) 113849

Contents lists available at ScienceDirect

Chaos, Solitons and Fractals

journal homepage: www.elsevier.com/locate/chaos

Diffusive pseudo-conformal mapping: Anisotropy-free transformation thermal media with perfect interface matching

Gaole Dai [a,*], Fubao Yang [b], Jun Wang [c,d], Liujun Xu [e], Jiping Huang [b]

[a] School of Sciences, Nantong University, Nantong 226019, China
[b] Department of Physics, State Key Laboratory of Surface Physics, and Key Laboratory of Micro and Nano Photonic Structures (MOE), Fudan University, Shanghai 200438, China
[c] School of Physics, East China University of Science and Technology, Shanghai 200237, China
[d] School of Mathematics, East China University of Science and Technology, Shanghai 200237, China
[e] Graduate School of China Academy of Engineering Physics, Beijing 100193, China

ARTICLE INFO

Keywords:
Diffusion
Heat transfer
Transformation theory
Pseudo-conformal mappings

ABSTRACT

Transformation media provide a fundamental paradigm for field regulation, but their tricky anisotropy challenges fabrication. Though optical conformal mapping has been utilized to eliminate anisotropy, two key factors still hinder its development in thermotics, i.e., the distinct diffusion nature and inevitable interface mismatching. Here, we put forth the concept of diffusive pseudo-conformal mapping, overcoming the inherent difference between diffusion and waves and achieving perfect interface matching. The proposed mapping directly leads to heat guiding and expanding functions with anisotropy-free transformation thermal media, whose feasibility is confirmed by experiments or simulations. Besides diverse applications, we provide a unified perspective for two distinct types of prevailing bilayer cloaks by uncovering their profound ties with pseudo-conformal mapping. These results greatly simplify the preparation of transformation thermotics and have implications for regulating other diffusion and wave phenomena.

Heat control is essential for every aspect of human life, such as energy utilization, chip cooling, and infrared detection. The past decade has witnessed the development of transformation theory [1,2] in heat conduction, a diffusion process that intrinsically differs from wave dynamics [3,4]. Transformation thermotics indicates that anisotropic and inhomogeneous thermal parameters in physical space can mimic heat transfer in curved space, ensured by the form-invariance of heat equations under coordinate transformations. However, anisotropy considerably restricts practical realization because natural materials usually exhibit isotropic thermal properties. Though alternative schemes like diffusive scattering cancellation were proposed to avoid anisotropy [5–8], they generally apply to specific scenarios such as thermal invisibility. Therefore, removing the intrinsic anisotropy of transformation thermal media is still a big challenge.

Conformal transformation optics [1,9] can eliminate anisotropy with two-dimensional (2D) optical conformal mapping that locally preserves the angles and orientations of curves [10]. Diverse wave phenomena have been realized with anisotropy-free transformation refractive index [11–19]. However, two critical problems challenge the application of optical conformal mapping in thermotics. On the one hand, diffusion and waves fundamentally differ in governing equations (i.e., the Laplace equation vs. the Helmholtz equation) and key parameters (i.e., thermal conductivity vs. refractive index). On the other hand, matching the interface heat flux between the functional device and background is still tricky due to the lack of intuitive impedance matching criteria, which is essential for accurate and robust heat manipulation. Thus, directly utilizing optical conformal mapping for precise diffusion control is impracticable.

Here, we propose the concept of diffusive pseudo-conformal mapping with angle preservation for certain families of curves representing thermal fields. Fortunately, "pseudo" does not affect the crucial advantage of "conformal" in removing anisotropy and contributes to perfect interface matching. The proposed mapping yields precise heat manipulation with anisotropy-free transformation thermal media, and we take heat guiding and expanding as two typical examples, with experimental or simulated confirmation. Moreover, we reveal the geometric origin of bilayer cloaks previously designed by scattering cancellation from the perspective of pseudo-conformal mapping. These results feature scalability in handling complex heat transfer [20–22] and provide a unified geometric perspective toward various thermal functions with isotropic materials.

* Corresponding author.
E-mail addresses: gldai@ntu.edu.cn (G. Dai), ljxu@gscaep.ac.cn (L. Xu), jphuang@fudan.edu.cn (J. Huang).

https://doi.org/10.1016/j.chaos.2023.113849
Received 17 June 2023; Accepted 15 July 2023

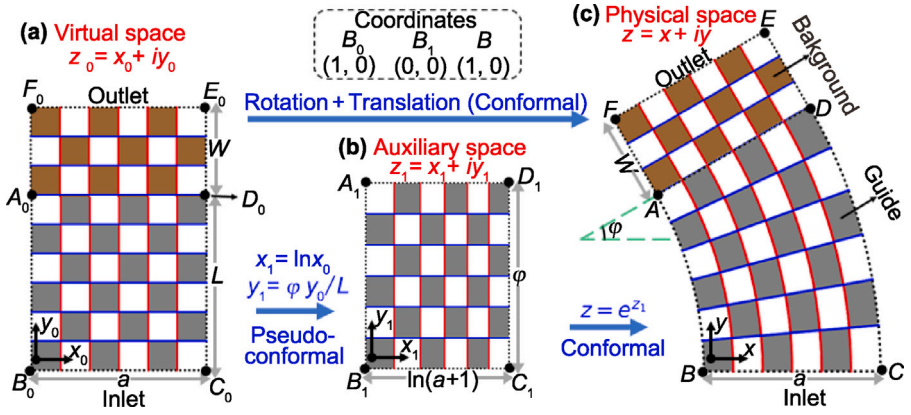

Fig. 1. Transformation for a heat flux guide (gray and white meshes) including the background (brown and white meshes). (a), (b) and (c) are the virtual space, the auxiliary space (only showing the transformation of the guide) and the physical space, respectively. (For interpretation of the references to color in this figure legend, the reader is referred to the web version of this article.)

For clarity, we first establish diffusive conformal mapping and illustrate its restrictions. A 2D conformal mapping $f : z_0 = x_0 + iy_0 \mapsto z = f(z_0) = x + iy$ satisfies the Cauchy–Riemann equations [10],

$$\frac{\partial f}{\partial \overline{z_0}} = \frac{1}{2}\left(\frac{\partial f}{\partial x_0} + i\frac{\partial f}{\partial y_0}\right) = 0, \tag{1}$$

where $\overline{z_0}$ is the complex conjugate of z_0. We consider form-invariant heat conduction equations in physical space (position denoted by z) and virtual space (position denoted by z_0),

$$\nabla \cdot (\boldsymbol{\kappa} \nabla T(z)) - Q = 0, \tag{2a}$$

$$\nabla_0 \cdot \left(\boldsymbol{\kappa}_0 \nabla_0 T_0(z_0)\right) - Q_0 = 0, \tag{2b}$$

where T, $\boldsymbol{\kappa}$, and Q are the temperature, thermal conductivity (rank-2 tensor), and internal source power in physical space, respectively. Their counterparts with a subscript "0" denote corresponding parameters in virtual space. The transformation rules to ensure $T(z) = T_0(f^{-1}(z_0))$ are [23,24]

$$\boldsymbol{\kappa}(z) = \mathrm{J}_f \boldsymbol{\kappa}_0(z_0) \mathrm{J}_f^{\mathrm{T}} / \det \mathrm{J}_f, \tag{3a}$$

$$Q(z) = Q_0(z_0) / \det \mathrm{J}_f, \tag{3b}$$

where J_f is the Jacobian of f and $\mathrm{J}_f^{\mathrm{T}}$ is its transpose. Under the conventional paradigm of transformation theory, the virtual space is isotropic and homogeneous. Further, $\mathrm{J}_f \mathrm{J}_f^{\mathrm{T}} / \det \mathrm{J}_f$ is an identity matrix under Eq. (1) [9], so κ and κ_0 are the identical constant scalar. This result is consistent with the conventional technique using conformal mapping to solve heat equations in irregular geometric domains [25]. Unlike the engineered gradient index in conformal transformation optics, such a frozen degree of freedom (i.e., $\kappa = \kappa_0$) restricts the function design for thermal manipulation. Besides, transformation media are often in contact with the background that undergoes trivial mapping without changing material properties. However, conformal mapping usually cannot ensure the continuity of boundary conditions due to the strict constraint of Eq. (1), i.e., conformality for all curves, as shown in the examples below. In fact, in most cases, we do not even have the option to consider interface matching due to the uniqueness of conformal mapping between two given domains. Therefore, we must develop diffusive pseudo-conformal mapping further and design thermal guiding and expanding functions.

Thermal guiding can bend the heat flux by an arbitrary angle. Its virtual space and physical space are shown in Figs. 1(a) and 1(c), respectively. In the virtual space, we apply a thermal bias along the y_0-axis. The inlet (hot source) is put on the bottom horizontal boundary B_0C_0 and the outlet (cold source) is on the top boundary F_0E_0. The vertical boundaries $F_0A_0B_0$ and $E_0D_0C_0$ are thermally insulated. In the physical space, we expect the flux to be rotated by angle φ when flowing out of the guide without changing its magnitude. In Fig. 1(a), we plot the grid lines of the Cartesian coordinates. They are the heat flux streamlines (constant-x_0 curves) and the isotherms (constant-y_0 curves). The upper rectangle (with a height W) undergoes a composition of rotation and translation to the background in Fig. 1(c) without changing its thermal conductivity. The lower rectangle (with a height L) is transformed into the partial annulus (the guide) in Fig. 1(c). Notably, an identity transformation should happen between the inlets B_0C_0 and BC. Also, the mappings for the background and the guide should have the same effect at their interface AD (on the constant-azimuth line equal to φ in Fig. 1(c), which is mapped from A_0D_0 in Fig. 1(a)). The other boundaries, FAB and EDC, are still insulated in the physical space. Although there exists a conformal mapping between the guide and its preimage according to Riemann mapping theorem [10], it generally cannot transform B_0C_0 (or A_0D_0) into BC (or AD), let alone achieve the interface effect as we want (see our discussion based on the theory of quasiconformal mapping in Supplemental Material, Note I [26]).

To construct the guide, a two-step approach is implemented. The conformal logarithmic mapping can induce a waveguide in optics [9]. Using its inverse, we can pull the physical space back into an intermediate named the auxiliary space (position denoted by $z_1 = x_1 + iy_1$). However, its boundary conditions (including shape and heat flux distribution) do not meet our expectations. We must pull the intermediate back into the virtual space with a non-conformal mapping to compensate. The key lies in how to determine such a transformation and its inverse. A notable feature of isotropic media is that the isotherms are orthogonal to the streamlines. The appropriate non-conformal mapping should maintain the orthogonality of these two families of curves. This corresponds to a class of transformations stretching/compressing the rectangle in virtual space along the Cartesian coordinate axes. We choose one from them that achieves interface matching. Based on the above considerations, the first step from the virtual space to the auxiliary space [Figs. 1(a) and 1(b)] is $x_1 = \ln x_0$, and $y_1 = \varphi y_0 / L$, and the second step to the physical space [Fig. 1(c)] is $z = \exp(z_1)$. Particularly, the composition transformation on the inlet $B_0C_0 \mapsto BC$ is an identity one. Also, its effect on the interface $A_0D_0 \mapsto AD$ is the same as the translation plus rotation the background undergoes. This guarantees that the interface matches. For an isotropic homogeneous virtual space, the thermal conductivities in the auxiliary space (denoted by $\boldsymbol{\kappa}_1$) is a real-valued symmetric tensor and can be diagonalized using Cartesian coordinates, writing $\boldsymbol{\kappa}_1 = \kappa_0 \mathrm{diag}\left(\frac{\partial x_1}{\partial x_0} / \frac{\partial y_1}{\partial y_0}, \frac{\partial y_1}{\partial y_0} / \frac{\partial x_1}{\partial x_0}\right)$, if we directly use the transformation rule [Eq. (3a)]. It is worth noting that the principal axes happen to be the isotherms and streamlines (or more generally, their tangents at each point), and only $\kappa_1^{y_1 y_1}$ contributes to heat flux. Similarly in the physical space, $\boldsymbol{\kappa}$ can also be diagonalized in the isotherm-streamline grids, and only the diagonal element along the

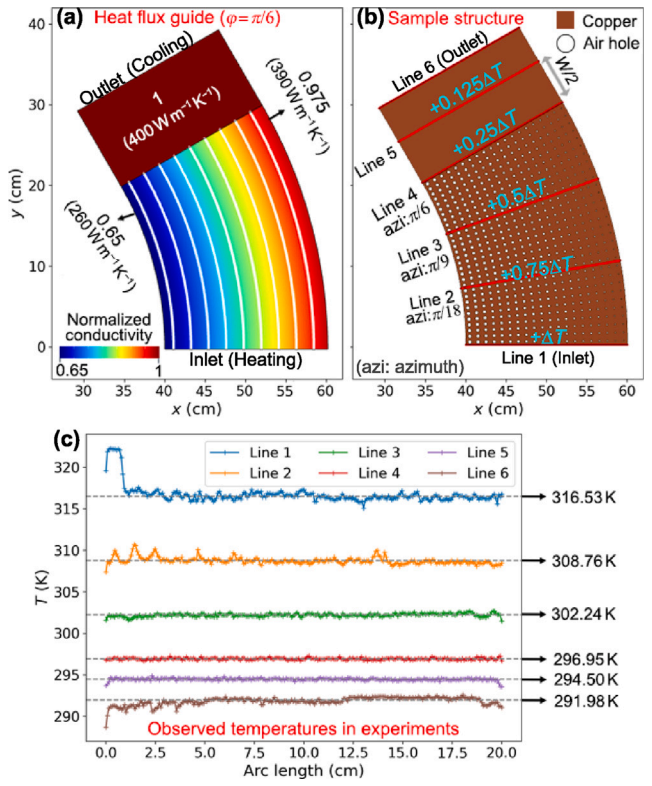

Fig. 2. (a) Normalized thermal conductivity (κ/κ_0) profile of the guide. The white curves are isolines. (b) Sample structure made of copper and air holes for experimental setup. (c) Measured temperatures showing the data on the red lines plotted in (b). The arc length means the distance from left endpoint. (For interpretation of the references to color in this figure legend, the reader is referred to the web version of this article.)

streamlines (equal to $\kappa_1^{y_1 y_1}(z_1)$ due to the conformality) can influence the heat transfer. A detailed explanation of such a diagonalization is presented in Supplemental Material, Note I [26], especially from Eq. (S5) to Eq. (S13). In this way, we can use isotropic media in these two spaces to realize the same effect by taking

$$\kappa(z) = \kappa_1(z_1(z)) = \kappa_0 \frac{\varphi}{L}\sqrt{x^2+y^2}. \tag{4}$$

We plot the grid lines in Figs. 1(b) and 1(c) mapped from their counterparts in Fig. 1(a). The three sets of grid lines are all orthogonal since they are streamlines and isotherms in their spaces. The streamlines in Figs. 1(a) and 1(c), which are both evenly distributed, so the heat flux magnitude is not changed. Also, the flux in the guide does turn an angle φ as expected. Intuitively, we call the first mapping "pseudo-conformal" for maintaining the orthogonality of certain curves. By doing a pseudo-conformal mapping first and then a conformal one, the composition is still pseudo-conformal. An alternative to make $\boldsymbol{\kappa}_1$ and $\boldsymbol{\kappa}$ isotropic is assuming $\boldsymbol{\kappa}_0 \sim \mathrm{diag}\left(\frac{\partial y_1}{\partial y_0}/\frac{\partial x_1}{\partial x_0}, \frac{\partial x_1}{\partial x_0}/\frac{\partial y_1}{\partial y_0}\right)$, which shall not change the thermal fields in any space, and we can directly obtain isotropic parameters based on Eq. (3a).

To confirm our design, we perform an experiment with the following parameters: $a = 0.5$, $L = 3W = \varphi/0.65$, $\varphi = \pi/6$ and $\kappa_0 = 400$ W m^{-1} K^{-1} (e.g., copper). Here, the unit length is 40 cm. Thermal conductivity based on Eq. (4) is shown in Fig. 2(a) and the background has the same value as κ_0. The inhomogeneous κ is approximated by a copper and air-hole composite [Fig. 2(b)]. We plot six straight lines, including the inlet (Line 1) and outlet (Line 6) in Fig. 2(b). Line 4 is the interface of the guide and background. Lines 2 and 3 divide the guide into thirds. Line 5 is in the middle of the background. Ideally, the temperature difference relative to the outlet on each line (isotherm) is marked in Fig. 2(b). The total thermal bias is ΔT, which is experimentally realized by water baths heating or cooling the sample. Fig. 2(c) shows the observed temperatures. Each of the six lines is roughly isothermal, and we plot horizontal lines corresponding to their mean value (excluding edge extremes). Notably, the temperature differences between Lines 4–6 are almost equal. We can conclude that the sample can bend the flux and keep its homogeneity. More details about the experimental setup and data are presented in Supplemental Material, Note II [26].

Next, we design a thermal expander that can convert the heat flux emitted by the point source into parallel flows. The virtual space [Fig. 3(a)] is the lower half-plane. The isotherms are concentric semi-circles with the point source at the center. To determine the temperature distribution, its value on a certain isotherm should be given, e.g., 290 K on $\{z_0 : |z_0| = 1, y \leqslant 0\}$ via an external source. The x_0-axis is thermally insulated except for the point source. By doing a conformal Möbius mapping $z = i\frac{i+z_0}{i-z_0}$ [9], the unit lower half-disk becomes the unit upper half-disk in the physical space [Fig. 3(b)]. The point source is now at $z = i$ and its power becomes $Q = Q_0/2$ to ensure $T(z) = T_0(z_0(z))$. The lower boundary on the x-axis $\{z : |x| \leqslant 1, y = 0\}$ is an isotherm (and also the external source) mapped from $\{z_0 : |z_0| = 1, y \leqslant 0\}$ and the heat flux on it is parallel (along the negative y-axis). However, flux magnitude varies depending on which azimuth it is mapped from. For practical applications, we want a homogenized flux so it can keep parallel in a rectangular extension attached to $\{z : |x| \leqslant 1, y = 0\}$ when the external source is moved to the bottom of the extension. This homogenization can be realized by a composite mapping $z = i\frac{i+z_1(z_0)}{i-z_1(z_0)}$. The first step $\mathrm{Arg}[z_1] = 2\arctan\left(\frac{\mathrm{Arg}[z_0]-2\pi}{\mathrm{Arg}[z_0]-\pi}\right)+2\pi$ is pseudo-conformal from the virtual space to the auxiliary space, and Arg denotes the argument (see Supplemental Material, Note III for how to construct this mapping [26]). The first step is a mapping between grid lines of polar coordinates while the second step still uses the Möbius transformation. Under the new transformation, the applied boundary conditions do not need to be changed compared to the conformal mapping. More importantly, the transformation of the lower boundary from virtual space (semicircle arc) to physical space (diameter) is uniform for the arc length, which can keep the uniformity of heat flux. Similar to the guide, orthogonality between isotherms and streamlines (grid lines of polar coordinates in the virtual space) is maintained, and $\boldsymbol{\kappa}_1$ (or $\boldsymbol{\kappa}$) can also be replaced by a scalar. The thermal conductivity in the expander is

$$\kappa(x,y) = \kappa_1\left(1+\sqrt{\frac{\left(x^2+y^2-1\right)^2}{x^4+2x^2\left(y^2+1\right)+\left(y^2-1\right)^2}}\right)^{-1}. \tag{5}$$

Since κ is still isotropic, the heat flux on the x-axis can keep parallel. In Fig. 3(c), we plot the thermal fields in the new physical space. The intersections of streamlines with the x-axis are now uniformly distributed, which differs from the case in Fig. 3(b). This is an intuitive representation of homogenization. We further compare the flux on the x-axis produced by the two mappings in Fig. 3(d). The theoretical results agree with the finite-element numerical ones from COMSOL Multiphysics (https://www.comsol.com/). In Supplemental Material, Note IV [26], we confirm the performance of our design when considering an extension. Eq. (5) can also be written in a compact form using transposed bipolar coordinates (See Supplemental Material, Note V [26]).

Besides functional design in different scenarios, our approach can also reveal the underlying ties between material parameters and coordinate transformations for some previous works based on alternative schemes of transformation theory. Here, for example, we provide a geometric insight into bilayer cloaks [5–8]. Transformation-based annular cloak (shell cloak) depends on a non-homeomorphic mapping to generate its inner boundary, e.g., transforming a point or a line into a closed curve [1,2]. Due to the geometric symmetry, we consider the upper half of an annular cloak, i.e., a carpet cloak. The virtual and physical spaces in Fig. 4 show a transformation from the upper half-disk

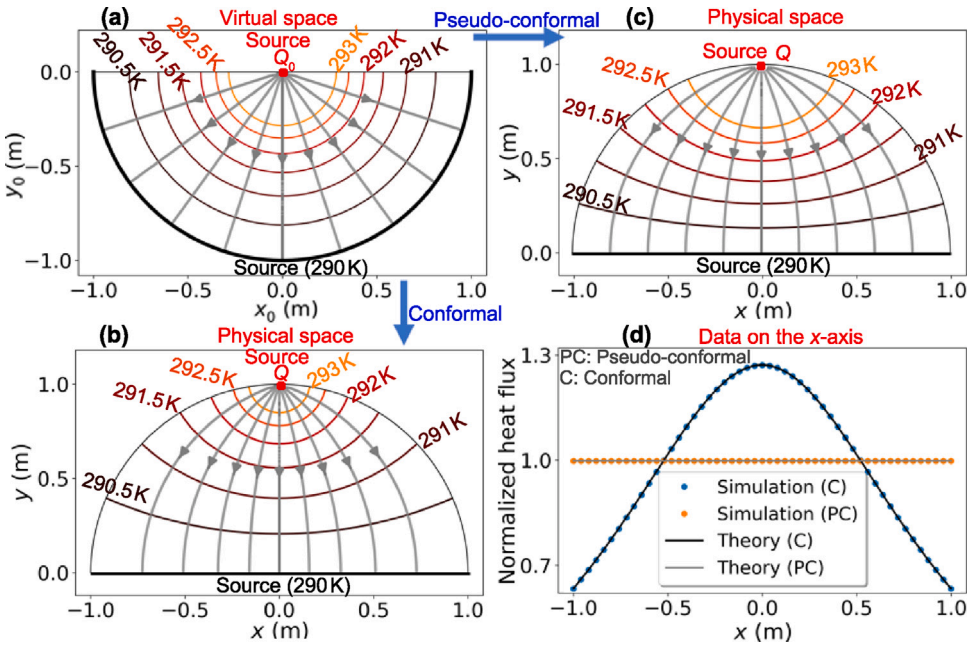

Fig. 3. Thermal expander. (a) The virtual space with the point source at the origin. Concentric semicircles are isotherms. Gray curves with arrows represent streamlines, which are also constant-azimuth lines ranging from 1.1π to 1.9π (0.1π interval from left to right). (b) The physical space for a conformal mapping. (c) The physical space for a pseudo-conformal mapping. The thermal fields in (a)–(c) are illustrated based on finite element numerical results. (d) The magnitude of the normalized heat flux on the x-axis for the two physical spaces. The solid lines are theoretical results while the scatter charts with markers are numerical results. Here, we take $\kappa_0 = 400$ W m^{-1} K^{-1} and $Q_0 = 3000$ W m^{-3}. (For interpretation of the references to color in this figure legend, the reader is referred to the web version of this article.)

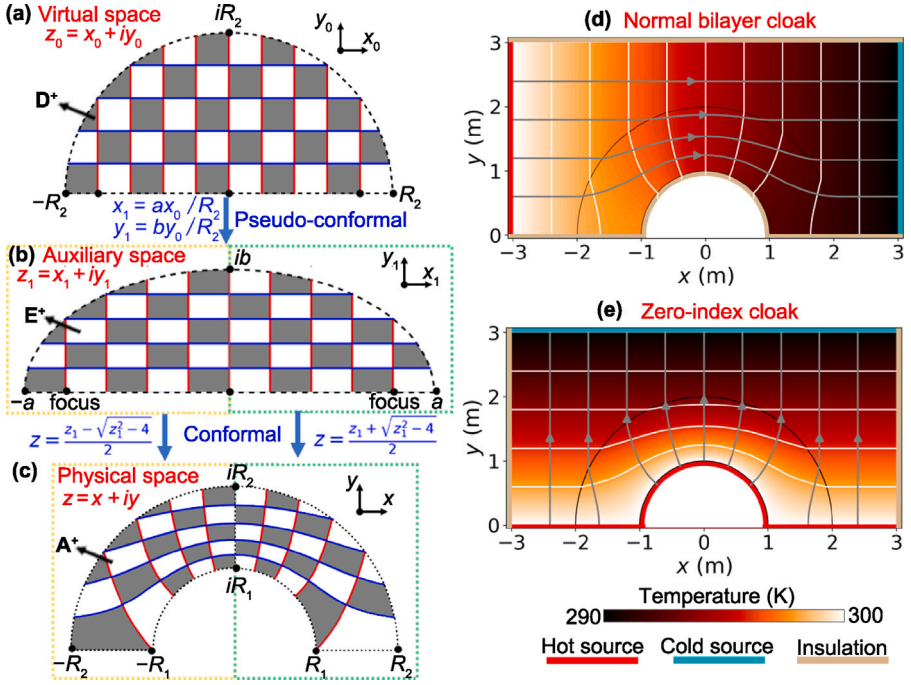

Fig. 4. Carpet cloaks. (a)–(c) show the geometric transformation to construct such a cloak. (a), (b), and (c) are the virtual space, auxiliary space and the physical space, respectively. (d) is the computed temperature profile of a normal bilayer cloak with an insulating inner layer. We place the hot source (300 K) and the cold source (200 K) on the left and right boundaries, respectively, generating a thermal bias along the x-axis. (e) is the computed temperature profile of a zero-index cloak with an constant-temperature inner layer (realized by an external source). We illustrate white curves for isotherms and gray curves with arrows for streamlines. Here, we take $R_2 = 2R_1 = 2$ m and $\kappa_0 = 400$ W m^{-1} K^{-1}. The entire simulation domain is limited to a 6 m × 3 m rectangle. (For interpretation of the references to color in this figure legend, the reader is referred to the web version of this article.)

$\mathbf{D}^+$ with a radius R_2 to the upper half-annulus $\mathbf{A}^+ = \{z : R_1 \leqslant |z| \leqslant R_2, y \geqslant 0\}$ [Fig. 4(c)]. Here $\mathbf{A}^+$ is actually the outer layer of a bilayer cloak. For simplicity, we take $R_1 = 1$ (in meters). The area outside $\mathbf{D}^+$ or $\mathbf{A}^+$ is the background. A cloak means the area enclosed by $\mathbf{A}^+$ is expected to have no disturbance to the background. We still use a two-step pseudo-conformal mapping. First, $\mathbf{D}^+$ is compressed/expanded into an half-ellipse $\mathbf{E}^+ = \{z_1 : 0 \leqslant x_1^2/a^2 + y_1^2/b^2 \leqslant 1, y_1 \geqslant 0\}$ [Fig. 4(b)] by $x_1 = \frac{a}{R_2} x_0$ and $y_1 = \frac{b}{R_2} y_0$. Here we take $a = (R_2^2 + R_1^2)/R_2$ and

$b = (R_2^2 - R_1^2)/R_2$ so the foci of the half-ellipse are $(\pm 2R_1, 0) = (\pm 2, 0)$. This non-conformal mapping is angle-preserving for the Cartesian grid lines in Fig. 4(a) so it is pseudo-conformal. Second, conformally map $\mathbf{E}^+$ to $\mathbf{A}^+$:

$$\begin{cases} z = \dfrac{z_1 - \sqrt{z_1^2 - 4}}{2}, & \text{if } x_1 < 0 \\ z = \dfrac{z_1 + \sqrt{z_1^2 - 4}}{2}, & \text{if } x_1 \geqslant 0. \end{cases} \tag{6}$$

This mapping is one branch of the inverse Zhukovsky transform [27] (See Supplemental Material, Note VI for detailed explanation [26]). In particular, the upper boundary of $\mathbf{A}^+$ (i.e., $\{z : |z| = R_2, y \geqslant 0\}$) finally undergoes an identity transformation as well as the background. If the thermal bias is applied along the x_0-axis, the grid lines in Fig. 4(a) represent horizontal streamlines and vertical isotherms, and we find the thermal conductivity in $\mathbf{A}^+$ is

$$\kappa = \frac{R_2^2 + R_1^2}{R_2^2 - R_1^2}\kappa_0, \tag{7}$$

which is the cloaking condition for the outer layer of a bilayer cloak [5]. In addition, the lower boundary of $\mathbf{A}^+$ including $\{z : |z| = R_1, y \geqslant 0\}$ and $\{z : R_1 \leqslant |x| \leqslant R_2, y = 0\}$ (denoted by Γ as a whole) are mapped from a streamline in the virtual space. The heat flux should have no normal component on Γ, which can be ensured by the insulation condition. This corresponds to the cloaking condition for the inner layer of a bilayer cloak, i.e., zero-value thermal conductivity and arbitrary shape as along as it covers $\{z : |z| = R_1, y \geqslant 0\}$.

If the thermal bias is instead along the y_0-axis, our mapping is still angle-preserving for the vertical streamlines and horizontal isotherms in Fig. 4(a). Now we take another diagonal element in the thermal conductivity and have

$$\kappa = \frac{R_2^2 - R_1^2}{R_2^2 + R_1^2}\kappa_0. \tag{8}$$

The lower boundary Γ is mapped from an isotherm, leading to another bilayer cloak made of zero-index materials [7]. We call the previous cloak "normal bilayer" to distinguish them. The term "zero-index" refers to the constant-temperature condition on the inner layer that can be replaced by an effectively infinite thermal conductivity [7,8]. Figs. 4(d) and 4(e) numerically confirm the performance of the two cloaks. In addition to the invisibility effect, we can see that the patterns of isotherms and streamlines in the two cloaks have a duality relationship by swapping the family of curves for streamlines and isotherms. Further, our mapping can be performed on the entire plane to build the shell cloak. Our method can be easily generalized to the transient case by further considering the transformation of density and specific heat and also be used to design invisibility devices with other geometries like confocally elliptical cloaks (See Supplemental Material, Notes VII and VIII for detailed discussions, respectively [26]).

In summary, we propose the concept of diffusive pseudo-conformal mapping to simultaneously achieve precise heat flux regulation and maintain the material isotropy in transformation thermotics. By preserving the orthogonality of certain families of curves (i.e., isotherms and streamlines) whose tangents behave as the principal axes for diagonalizing thermal conductivity tensor, our approach can circumvent material anisotropy and perfectly match the interface heat flux between the transformation media and background. We demonstrate our theory by designing feasible and robust thermal devices that can bend or parallelize heat flux at our will. Also, we revisit scattering-cancellation-based bilayer cloaks from a unified perspective of pseudo-conformal mapping. In addition to reobtaining the parameters without inversely solving heat equations, the intrinsic geometric relationship between different types of bilayer cloaks is also revealed. The idea of diffusive pseudo-conformal mapping can be further developed for controlling transient heat conduction [24,28], multithermotics [29,30], and other diffusion physics [31–34]. The consideration of perfect interface matching also benefits the design of transformation wave media, such as avoiding impedance mismatch that plagues conformal invisibility devices [35].

Declaration of competing interest

The authors declare that they have no known competing financial interests or personal relationships that could have appeared to influence the work reported in this paper.

Data availability

Data will be made available on request.

Acknowledgments

We acknowledge financial support from the National Natural Science Foundation of China (Grants No. 11725521, No. 12035004, No. 12147169, and No. 12205101) and the Science and Technology Commission of Shanghai Municipality, China (Grant No. 20JC1414700).

Appendix A. Supplementary data

Supplementary material related to this article can be found online at https://doi.org/10.1016/j.chaos.2023.113849.

References

[1] Leonhardt U. Science 2006;312:1777.
[2] Pendry JB, Schurig D, Smith DR. Science 2006;312:1780.
[3] Li Y, Li W, Han T, Zheng X, Li J, Li B, et al. Nat Rev Mater 2021;6:488.
[4] Yang S, Wang J, Dai G, Yang F, Huang J. Phys Rep 2021;908:1.
[5] Han T, Bai X, Gao D, Thong JTL, Li B, Qiu C-W. Phys Rev Lett 2014;112:054302.
[6] Xu H, Shi X, Gao F, Sun H, Zhang B. Phys Rev Lett 2014;112:054301.
[7] Li Y, Zhu K-J, Peng Y-G, Li W, Yang T, Xu H-X, et al. Nature Mater 2019;18:48.
[8] Xu L, Yang S, Huang J. Europhys Lett 2020;131:24002.
[9] Xu L, Chen H. Nat. Photonics 2015;9:15.
[10] Stein EM, Shakarchi R. Complex analysis. Princeton: Princeton University Press; 2003.
[11] Leonhardt U, Tyc T. Science 2009;323:110.
[12] Huang Y, Zhang Y, Zhang J, Liu D, Wang Q, Zhang B, et al. Nanophotonics 2020;9:3243.
[13] Kraft M, Luo Y, Maier SA, Pendry JB. Phys Rev X 2015;5:031029.
[14] Chen Q, Horsley SAR, Fonseca NJG, Tyc T, Quevedo-Teruel O. Nature Commun 2022;13:2354.
[15] Wang X, Chen H, Liu H, Xu L, Sheng C, Zhu S. Phys Rev Lett 2017;119:033902.
[16] Kim Y, Lee S-Y, Ryu J-W, Kim I, Han J-H, Tae H-S, et al. Nat. Photonics 2016;10:647.
[17] Liu Y, Sun F, Yang Y, Chen Z, Zhang J, He S, et al. Phys Rev Lett 2020;125:207401.
[18] Xu L, He R, Yao K, Chen JM, Sheng C, Chen Y, et al. Phys Rev A 2019;11:034072.
[19] Lu L, Ding K, Galiffi E, Ma X, Dong T, Pendry JB. Nature Commun 2021;12:6887.
[20] Li Y, Shen X, Wu Z, Huang J, Chen Y, Ni Y, et al. Phys Rev Lett 2015;115:195503.
[21] Yang F, Xu L, Wang J, Huang J. Phys Rev A 2022;18:034080.
[22] Dai G, Shang J, Huang J. Phys Rev E 2018;97:022129.
[23] Fan C, Gao Y, Huang J. Appl Phys Lett 2008;92:251907.
[24] Guenneau S, Amra C, Veynante D. Opt Express 2012;20:8207.
[25] Naterer GF. Advanced heat transfer. 3rd.. Boca Raton: CRC Press; 2022.
[26] See Supplemental Material which includes Refs. [5,10,24,27,36–45].
[27] Brown JW, Churchill RV. Complex variables and applications. 9th.. New York: McGraw-Hill Education; 2014.
[28] Xu L, Liu J, Jin P, Xu G, Li J, Ouyang X, et al. Natl Sci Rev 2022;nwac159.
[29] Xu L, Huang J. Phys Rev A 2019;12:044048.
[30] Dai G, Zhou Y, Wang J, Yang F, Qu T, Huang J. Phys Rev A 2022;17:044006.
[31] Schittny R, Kadic M, Bückman T, Wegener M. Science 2014;345:427.
[32] Ma Y, Liu Y, Raza M, Wang Y, He S. Phys Rev Lett 2014;113:205501.
[33] Gömöry F, Solovyov M, Šouc J, Navau C, Prat-Camps J, Sanchez A. Science 2012;335:1466.
[34] Jiang W, Ma Y, He S. Phys Rev A 2018;9:054041.
[35] Xu L, Chen H, Tyc T, Xie Y, Cummer SA. Phys Rev B 2016;93:041406, (R).
[36] Ahlfors LV. Lectures on quasiconformal mappings. 2nd.. Providence: American Mathematical Society; 2006.
[37] Alberge V, Papadopoulos A. In: Papadopoulos A, editor. Handbook of teichmüller theory, Vol. VII. Zürich: European Mathematical Society; 2020, p. 393–415.
[38] Li J, Pendry JB. Phys Rev Lett 2008;101:203901.
[39] Liu R, Ji C, Mock JJ, Chin JY, Cui TJ, Smith DR. Science 2009;323:366.
[40] Zhang B, Chan T, Wu B-I. Phys Rev Lett 2010;104:233903.

[41] Zhang J, Pendry JB, Luo Y. Adv. Photonics 2019;1:014001.
[42] Zeng W, Lui LM, Luo F, Chan TF-C, Yau S-T, Gu DX. Numer Math 2012;121:671.
[43] Markel VA. J Opt Soc Amer A 2016;33:1244.
[44] Han T, Yang P, Li Y, Lei D, Li B, Hippalgaonkar K, et al. Adv Mater 2018;30:1804019.
[45] Qin J, Luo W, Yang P, Wang B, Deng T, Han T. Int J Heat Mass Transfer 2019;141:487.